Polymer Chemistry

A General Model for the Ideal Chain Length Distributions of Polymers Made with Reversible Deactivation

Journal:	*Polymer Chemistry*
Manuscript ID	PY-ART-10-2021-001331.R1
Article Type:	Paper
Date Submitted by the Author:	28-Dec-2021

Complete List of Authors:	Kearns, Madison; Miami University, Department of Chemistry and Biochemistry Morleey, Colleen; Miami University, Department of Chemistry and Biochemistry Parkatzidis, Kostas; ETH Zurich - D-MATL, Material Science ; ETH Zurich Whitfield, Richard; ETH Zurich - D-MATL, Sponza, Alvaro; Stony Brook University Chakma, Progyateg; Miami University, Department of Chemistry and Biochemistry De Alwis Watuthanthrige, Nethmi; Miami University, Department of Chemistry and Biochemistry Chiu, Melanie; Stony Brook University, Chemistry Anastasaki, Athina; ETH Zürich, Konkolewicz, Dominik; Miami University, Department of Chemistry and Biochemistry

A General Model for the Ideal Chain Length Distributions of Polymers Made with Reversible Deactivation

Madison M. Kearns[a,†], Colleen N. Morley[a, †], Kostas Parkatzidis,[b] Richard Whitfield,[b] Alvaro D. Sponza,[c] Progyateg Chakma,[a] Nethmi De Alwis Watuthanthrige[a], Melanie Chiu[c], Athina Anastasaki[b], and Dominik Konkolewicz[a,*]

a Department of Chemistry and Biochemistry, Miami University, 651 E High St, Oxford, OH, 45056.

b Laboratory for Polymeric Materials, Department of Materials, ETH Zürich, Vladimir-Prelog-Weg 5, 8093 Zürich, Switzerland
c Stony Brook University, Department of Chemistry, Stony Brook, NY, 11794 USA

† Authors contributed Equally

* Correspondence: d.konkolewicz@miamiOH.edu

Abstract

Polymer molecular weight, or chain length distributions, are a core characteristic of a polymer system, with the distribution being intimately tied to the properties and performance of the polymer material. A model is developed for the ideal distribution of polymers made using reversible activation/deactivation of chain ends, with monomer added to the active form of the chain end. The ideal distribution focuses on living chains, with the system having minimal impact from irreversible termination or transfer. This model was applied to ATRP, RAFT, and cationic

polymerizations, and was also used to describe complex systems such as blended polymers and block copolymers. The model can easily and accurately be fitted to molecular weight distributions, giving information on the ratio of propagation to deactivation, as well as the mean number of times a chain is activated/deactivated under the polymerization conditions. The mean number of activation cycles per chain is otherwise difficult to assess from conversion data or molecular weight distributions. Since this model can be applied to wide range of polymerizations, giving useful information on the underlying polymerization process, it can be used to give fundamental insights into macromolecular synthesis and reaction outcomes.

Introduction

Polymerizations are powerful processes that can generate macromolecules with molecular weights well into the millions. In the past few decades, polymerizations subject to reversible activation and deactivation have received significant attention, as they allow polymers with living-like characteristics to be made under a range of reaction conditions,[1-3] including radical and cationic polymerizations.[4] This ability to reversibly activate a chain from a dormant state to a propagating chain end capable of adding monomer, with efficient reformation of the dormant form of the chain, enables well-controlled polymers to be formed, with clearly defined end-group control over the chain length. However, within this process of reversible activation and deactivation, there also is substantial kinetic information on the history of the chains, and this dictates the shape of the molecular weight distribution, as well as its moments, such as average chain lengths and the ratio of moment that gives chain length dispersity.[5] Developing kinetic models can both predict the shapes of molecular weight distributions, or conversely extract useful

information from experimental distributions, such as relative rates of propagation and deactivation or mean number of times a chain has been activated.[6-8]

Modeling is a useful tool to guide understanding of processes at the microscopic and submicroscopic levels in chemical systems and serve as predictive tools. There have been many publications in the field of polymer modeling, but many are limited by either the type of systems they can accurately predict and/or a lack of experimental data. Arguably, the simplest type of polymer modeling is a scaling model or scaling law that requires fewer input parameters, and relies on a greater number of assumptions.[9, 10] Such scaling laws or scaling models can provide trends and evaluate the impact of experimental variables on polymer properties or performance. For instance, scaling laws have been applied to predict the impact of radical initiator concentration on the polymerization rates of reactions such as reversible addition-fragmentation chain transfer (RAFT),[11, 12], or photoinduced electron/energy transfer RAFT (PET-RAFT).[13] Scaling laws have also been applied to activator complexes, deactivator complexes and alkyl halide in atom transfer radical polymerization (ATRP),[14-16] as well as radical initiators for continuous activator regeneration (ICAR) ATRP.[17] Similar equations exist to predict parameters, such as number average molecular weight or dispersity, as a function of initiator or deactivator.[1] Other 'simple' models for network formation created by Tobita and Hamielec, were designed when previous statistical theories were unsatisfactory.[18] The model applies a pseudokinetic rate constant to generate models for both pre- and post-gelation periods. However, this scaling law approach is unable to describe many important experimental features, such as the shape of the molecular weight distribution, fraction of uninitiated chains, or the properties of more complex polymers, like block copolymers or blended polymers.

At the other end of the spectrum, advanced and highly parameterized models have been developed. These models break out complex reactions into their elementary steps, associating each with a rate coefficient or equilibrium constant. Examples of such full kinetic modelling include PREDICI models applied to RAFT and ATRP,[19-22] methods of moments approaches to RAFT and ATRP,[23, 24] multichambered models for electrochemically mediated ATRP,[25] ATRP simulations in the presence of Cu^0,[26, 27] photochemical reactions,[28] and detailed models for retardation in RAFT polymerization.[29-35] Such detailed kinetic models have the ability to provide excellent insights into the underlying chemical processes, and can enable discrimination between several proposed pathways for polymerization processes and chemical transformations. However, the large number of kinetic parameters requires either substantial fitting of theory to experimental data, or a very large number of model experiments carefully designed to extract key parameters.[26, 27, 36-38] Coupling kinetic modelling with quantum chemistry can lead to many important insights and can either bypass or supplement model experiments;[39-44] however, quantum calculations can also be computationally expensive, especially for larger systems, such as polymers.

The last type of modeling in the polymer field lies in between the complex and simple models. These types of models use a limited number of parameters to predict kinetic data or products of a reaction. In addition, fewer experiments are needed to verify the model than in a complex model. However, such models can provide substantially more information than simple scaling laws.

In the case of polymerizations subject to reversible deactivation, several related models have been developed. For instance, Tobita developed a model for the molecular weight or chain length distribution of polymers made with reversible deactivation radical polymerization (RDRP).[45, 46] Goto and Fukuda considered kinetic models for the distribution of polymers made by of nitroxide

mediated polymerization[47] which could be adapted to other approaches.[1] Harrisson used a model based on intermittent activation and deactivation in RDRP to predict the chain length distribution of polymers made under various conditions.[48] This model uses assumptions to simplify calculations, but the distributions can be graphed and understood easily.[48] A model for the chain length distribution was developed to describe the reversible activation deactivation processes in RAFT polymers[49]. This model was based on the mean number of activation cycles that the polymer chain undergoes (μ_{decap}), the probability of the chain being activated, the likelihood of adding a given number of monomers in an activation cycle as the ratio of propagation to deactivation rate coefficients (k*), and the targeted degree of polymerization. The presence of side reactions (termination and irreversible chain transfer) may result in significant deviations from the ideal case. Although these models are based on relatively simple and well-understood concepts, such as reversible deactivation, and addition of monomer to an active chain end, these models have not been broadly applied to a range of polymer systems.

In earlier work, a model for RAFT was developed and applied to short polymers.[49] However, broad testing of such a model against a range of complex polymerizations and macromolecules with complex structures has not been performed. Here, a MATLAB approach is taken, where experimental data can be input, and the model matched to the experimental molecular weight distribution, mean and molar mass dispersity. Trends within the model and limitations of the model are considered, and the model is applied to a range of polymerization methods including: RAFT targeting tunable dispersities,[50] PET-RAFT systems,[51] photochemical ATRP,[52] and cationic polymerization,[53] since each reaction is governed by reversible deactivation.[54] Additionally, one of the advantages of RDRP and other living-like polymerization is the ability to form block copolymers. Therefore this model is extended to more complex systems including block

copolymers,[51, 55, 56] and polymers with tailored molecular weight distributions made by blending two distinct polymers together.[57]

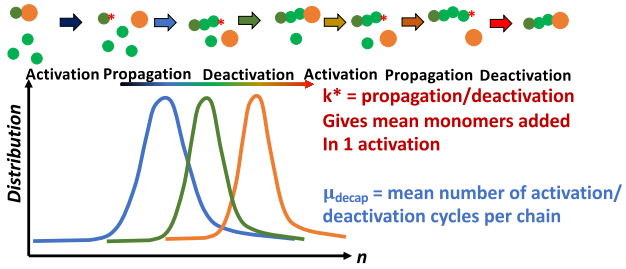

Scheme 1. Schematic description of polymerization with intermittent activation-deactivation cycles, and the parameters that govern the resulting chain length distribution.

Results and Discussion

Modeling Approach and Connection to Experimental Data

The modelling approach is given in the theoretical section. The model takes advantage of the reversible activation and deactivation of chains that occurs in the studied polymerizations, to predict polymer molecular weight distributions. Experimental parameters of mean chain length (DP_n), dispersity ($Đ$) and the size exclusion chromatography distribution ($w(logn)$) are used in conjunction with known values such as concentration of monomer $[M]_0$, concentration of chain initiator or reversible chain transfer agent [P–X] and deactivator concentration [D]. When comparing to experimental size exclusion chromatography data, band broadening is not explicitly accounted for in this model,[58, 59] but could be included with a subsequent broadening function, although this would increase the complexity of the model. The model is parameterized by two free parameters k^*, the ratio of propagation to deactivation rate coefficients, and μ_{decap}, the mean number of decapping events. These two parameters, k^* and μ_{decap}, are fitted to the experimental DP_n, $Đ$ and $w(logn)$ to obtain estimates of the ratio of propagation to deactivation rates and

number of activation-deactivation cycles. The modelling approach here, captures all kinetic effects such as temperature or reaction time within the parameters k^* and μ_{decap}, simplifying the system in the process.

Behavior of the model and sensitivity to model parameters

The theoretical section shows that the mean (DP_n), dispersity ($Đ$) and distributions ($w(logn)$) are functions of two model parameters, k^* and μ_{decap}, as well as experimental variables such as monomer, chain-end and deactivator concentrations. Therefore, it is essential to explore how these two model parameters k^* and μ_{decap} impact the outcomes of the model, before applying the model to a wide range of experiments. In particular, correlations of these two parameters must be explored, to ensure that meaningful and unique fits to the experimental data are possible.

Figure 1 demonstrates the changes in the model molecular weight distribution when μ_{decap} and k^* are altered. The top row of Figure 1 considers the number distribution, $p(\log n)$, while the bottom row shows the corresponding weight distribution, $w(\log n)$. The $w(\log n)$ curves correspond to the distributions derived from size exclusion chromatography under ideal conditions. Both the $p(\log n)$ and the $w(\log n)$ curves are normalized to a peak height of 1 as is commonly done in experimental work. Alternative approaches to normalization of the various polymer chain length and molecular weight distributions exist,[60] although the peak height comparison method allows rapid qualitative comparison between different simulated polymers. Quantitative comparison however, would be better performed by area normalization as outlined in recent work,[60] although the focus of Figure 1 is qualitative analysis. With a constant k^* of 0.1, the increase in μ_{decap} decreased the dispersity, narrowing the curve. As the μ_{decap} increased, the degree of polymerization increased, shifting the curve to the right in Figure 1a and 1b. The larger number of decapping events at a constant ratio of propagation to deactivation allows chains to continue to grow longer.

With subsequent decapping events, chains which lagged behind after just one or two decapping events are able to grow. Although the chains that were shorter after one to two decapping events will likely have a lower chain length after subsequent decapping events, the relative discrepancy in chain length between shorter and longer chains decreases with more decapping events. This leads to an overall shift in the distribution to longer chain length and overall lower dispersities, as seen in Figure 2a. Of particular note is that after just one or two decapping events, there is a substantial fraction of unreacted initiator, found at chain length 1, which is particularly pronounced in the number distribution, but somewhat obscured in the weight distribution.

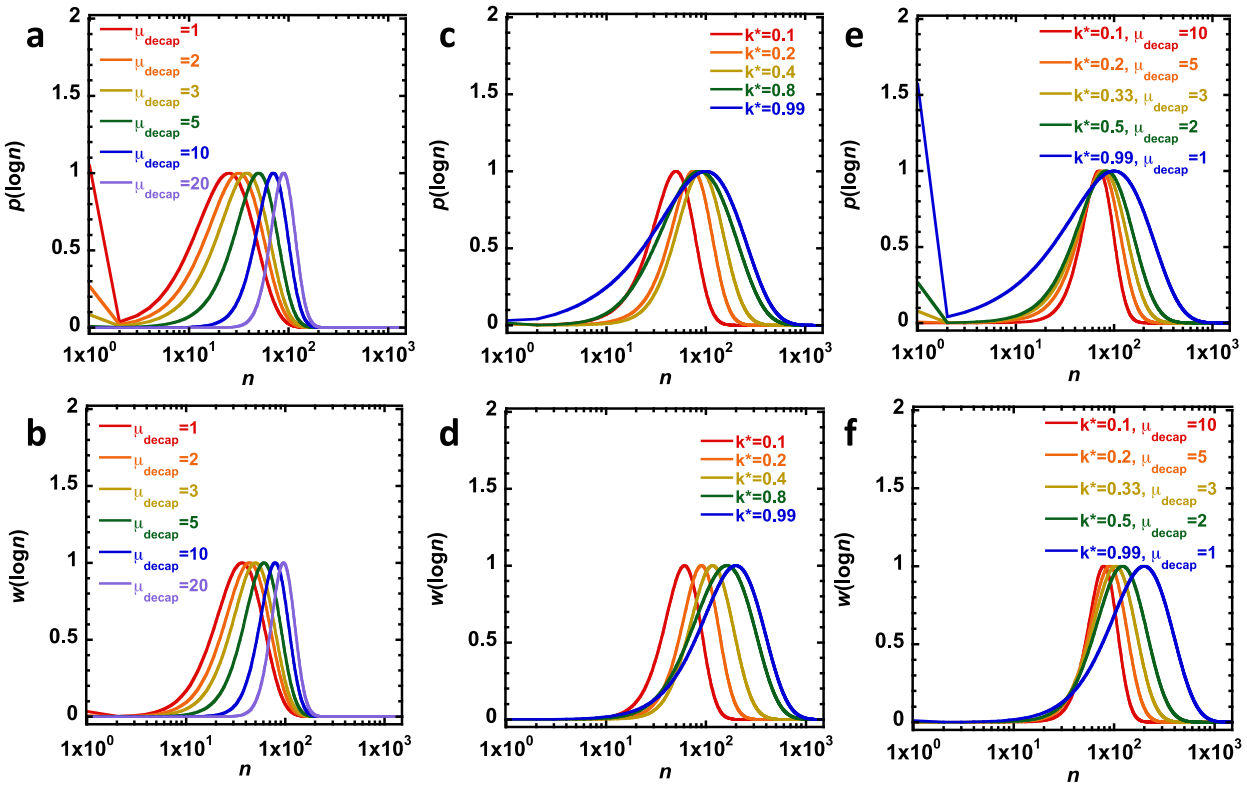

Figure 1. a) $p(\log n)$ distributions with constant $k^* = 0.1$ with changing μ_{decap}. b) $w(\log n)$ distributions with constant $k^* = 0.1$ with changing μ_{decap}. **c)** $p(\log n)$ distributions with constant $\mu_{decap} = 5$ with changing k^*. **d)** $w(\log n)$ distributions with constant $\mu_{decap} = 5$ with changing k^*. **e)**

$p(\log n)$ distributions with constant product of $k^* \times \mu_{decap} = 1$. **f)** $w(\log n)$ distributions with constant product of $k^* \times \mu_{decap} = 1$. In all cases $[M]_0 = 4$ M, [P-X] = [D] = 0.04 M.

At a constant μ_{decap} of 5, the increase in k^* increased the degree of polymerization and the dispersity. The curves broadened and shifted to the right in Figure 1c and 1d. This is due to the higher ratio of propagation to deactivation leading to more monomers being added per activation cycle. This results in both a higher degree of polymerization at a constant mean number of decapping events, but also a broader distribution, as seen in Figure 2b. The latter stems from the idea that more monomers added per decapping also lead a higher variability of monomers added per chain, since this deviates further from the ideal reversible deactivation polymerization where many activation-deactivation cycles are performed with only a few monomers added per cycle.

In Figure 1e and 1f, both k^* and μ_{decap} are varied while maintaining a constant product of near unity. As k^* increased and μ_{decap} decreased, the dispersity increased, while the mean degree of polymerization remained close to constant. This can be most clearly seen in the number distribution $p(\log n)$ in Figure 1e, where higher k^* and lower μ_{decap} leads to broadening of the distribution while maintaining the peak at approximately the same chain length, as seen in Figure 2c. Additionally, with just one or two decapping events on average, there remains a substantial amount of unreacted initiator at chain length 1, which is clearly visible in the number distribution, but obscured in the weight distribution due to the dominance of the higher chain length polymers. The results in Figure 1e and 1f show that both the product and absolute value of k^* and μ_{decap} are important in the distribution shape. The product of the two values contributes to the breadth of the curve, while the absolute value shifts the curve right or left. This implies that unique solutions can

be found by solving for absolute value of either k^* and μ_{decap} to match the mean chain length, with the of k^* and μ_{decap} varied to match the breadth of the distribution as quantified by the dispersity.

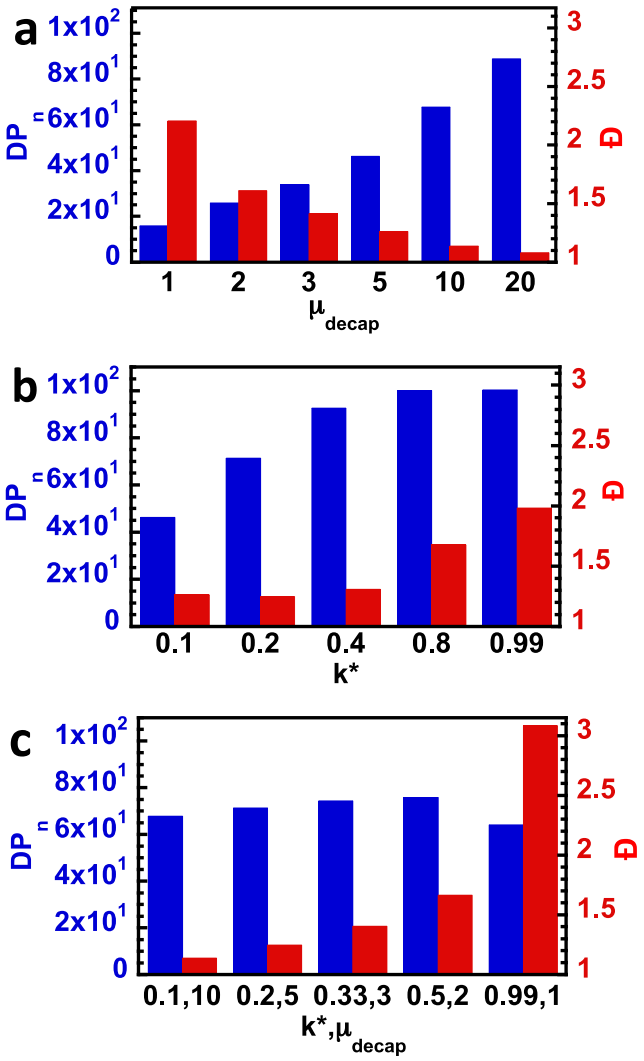

Figure 2. a) DP_n and $Đ$ with constant $k^* = 0.1$ and changing μ_{decap} **b)** DP_n and $Đ$ with constant $\mu_{decap} = 5$ with changing k^*. **c)** DP_n and $Đ$ with constant product of $k^* \times \mu_{decap} = 1$. In all cases $[M]_0 = 4$ M, [P-X] = [D] = 0.04 M.

The general trends observed in Figures 1 and 2 are that both k^* and μ_{decap} increase the average chain length, DP_n, towards the targeted chain length of $[M]_0/[P\text{-}X]+1$, and that higher k^*

values correlate with generally broader distributions. The advantages of the approach developed here are that the whole distribution is evaluated and predicted, rather than just moments of the distribution such as the mean or variance, the latter of which is correlated with the dispersity.[61] Figure S1 compares the results of this model, against the predictions of existing equations for dispersity:

$$Đ = 1 + \frac{1}{DP_n} + \left(\frac{2 - conversion}{conversion}\right)\left(k^* \frac{[P - X]}{[D]}\right) \quad (1)$$

In all cases the product of k^* and μ_{decap} was sufficiently large that the model predicts $DP_n \approx [M]_0/[P\text{-}X]+1$, allowing the polymerization to be considered near quantitative and conversion≈1. In general the model correctly predicted chain length as a function of the ratio $[M]_0/[P\text{-}X]$, indicating that the model is able to correctly identify the polymer's average chain length. Comparing the predictions of the developed model with those of equation 1 as given in Figure S1. The developed model tends to predict somewhat lower dispersities than those predicted by equation 1 across a range of systems. These include RAFT where the k* value is altered, ATRP where the deactivator and k* is altered and cationic where chain length and k* is varied. In general the discrepancy is relatively small, often comparable to experimental uncertainties, and is especially small at the extremes of low dispersity (Đ≈1) and high dispersity (Đ≈2). Since the general trends of the model developed in this work and the established approaches outlined by Goto et al. are similar, the developed model is subsequently applied to a range of polymer systems.

Application to RAFT Polymerization.

Recently, a general approach to synthesize RAFT polymers with tunable dispersity has been developed.[50, 51] This approach combines a chain transfer agent (CTA) exhibiting a high transfer constant with a RAFT agent that has a relatively low transfer constant. In this scenario, a

system with a high transfer constant should have a low k^* value, since in RAFT, the deactivation occurs through the degenerative transfer mechanism in Equations 2 and 3. In RAFT systems k^* is essentially the reciprocal of the apparent RAFT transfer constant.[1] Scheme 2 shows the RAFT polymerization of methyl acrylate (MA) and methyl methacrylate (MMA) in the presence of CTAs capable of giving low dispersity and high dispersity for each monomer. Note that in both cases, the medium dispersity polymer is generated by combining a 0.35 fraction of the CTA that gives low dispersity and 0.65 fraction of the CTA that gives the high dispersity polymers. Figure 3a and 3b demonstrate good agreement between the experimental chain length distribution data, derived from SEC, and the model for both MA and MMA systems. This agreement was good for the system targeting low dispersity, high dispersity, and a mixed CTA system that led to intermediate dispersity.

Interestingly, the medium-dispersity polymer, which is made with a mixture of an active CTA leading to narrow chain length distributions and a low-activity CTA leading to broad chain length distributions, could be approximated by a convolution of a polymer made under the conditions for the narrow and the broad fits to as seen in Figure S2. The direct fit of the medium dispersity data set by varying k^* and μ_{decap} given in Figure 3a. In the convolution approach, since the medium dispersity polymer was made with a fraction of 0.35 of the high activity CTA, and 0.65 of the low activity CTA, two polymer chain length distributions were simulated. The first polymer used the same k^* and μ_{decap} as the narrow MMA RAFT in Table 1, but targeted a chain length 35% of the medium dispersity chain length. The other polymer used the same k^* and μ_{decap} as the broad MMA RAFT in Table 1 but targeted a chain length 65% of the medium dispersity chain length. These two were convolved as outlined in the supporting information and gave acceptable agreement with the experimental chain length distribution. This convolution is used to

capture the fact that a polymer can switch from high to low activity chain end multiple times during the polymerization with mixed RAFT agents. However, the agreement between the convolved curve and the experiment was poorer than the one where the model was fit with an average k^* and μ_{decap} to the experiment, as shown in Figure S2. Therefore, in all future cases, the RAFT system is fit with k^* and μ_{decap} and [P-X]=[D]=[CTA], where [CTA] is the sum of all CTAs in the reaction medium.

RAFT

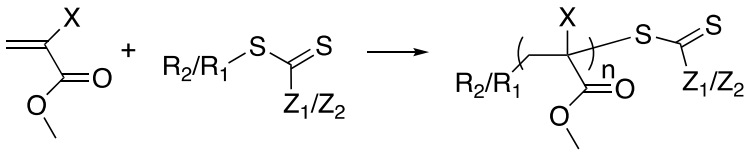

PET-RAFT

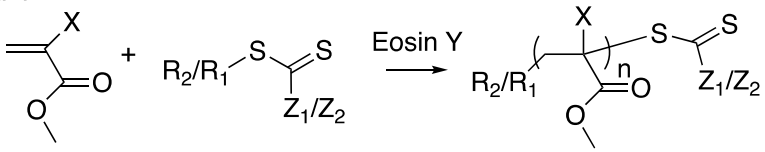

X = CH_3

High Activity

R_1 = 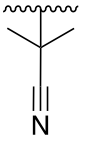

Z_1= 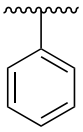

X = CH_3

Low Activity

R_2 = 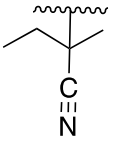

Z_2 = 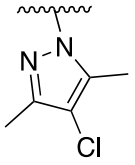

X = H

High Activity

R_1 = 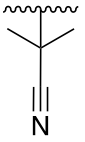

Z_1 = 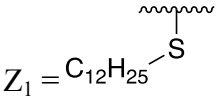

X = H

Low Activity

R_2 = 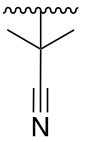

Z_2 = 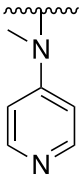

Scheme 2. RAFT polymerization of MMA and MA using thermal RAFT and PET-RAFT polymerization in the presence of CTAs with distinct activity. Note the medium dispersity system used a 0.35 fraction of the high activity CTA and 0.65 fraction of the low activity CTA in each case.

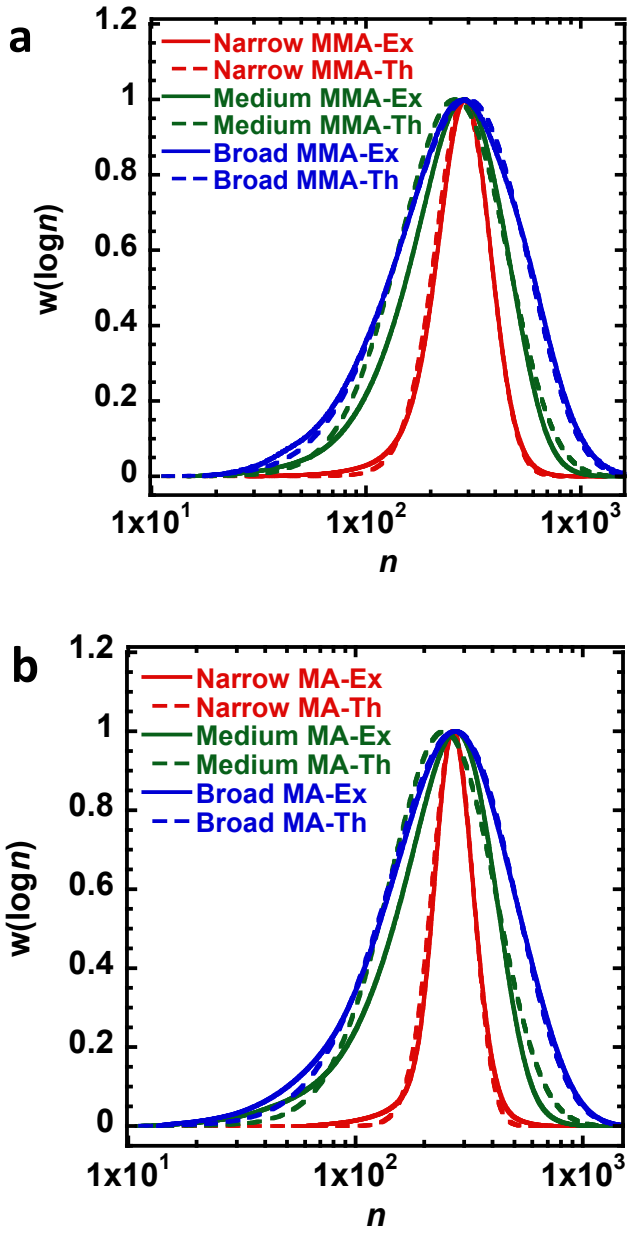

Figure 3. a) Molecular weight distributions from the PMMA thermal-RAFT polymer system and model predictions. **B)** Molecular weight distributions from the PMA thermal-RAFT polymer system and model predictions.

As seen in Table 1, k^* increased as the dispersity increased for both the RAFT MA and MMA polymer systems. The increase in k^* is perfectly in line with the anticipated changes in the RAFT transfer constant. Systems with high RAFT transfer constants, which leads to small values of k^*, should give narrow molecular weight distributions. Conversely, a low transfer constant leads to a high value of k^*, and leads to many monomers added in one activation cycle and broad molecular weight distributions. Interestingly, the k^* value for the medium dispersity system is similar to taking a weighted average of 0.35 of the narrow and 0.65 of the broad k^*, consistent with loading of the more active and less active CTAs used.

As the dispersity and k^* values increased, the μ_{decap} for the MA system decreases. This is consistent with the predictions in Figure 2c. However, this same trend is not observed for the MMA system. The medium dispersity distribution had a higher μ_{decap} than the narrow dispersity distribution. This diversion from the trend can be attributed to the relationship between conversion, chain length, and μ_{decap}. The MMA medium dispersity system reached 99% conversion, while the MMA low dispersity system only reached 83% conversion.[50] Since μ_{decap} increases with reaction time and conversion, the observed μ_{decap} value for the MMA medium dispersity system can be interpreted as a system that simply was allowed to reach higher conversion, and thereby requiring the chain to undergo more activation deactivation cycles. As the μ_{decap} increases, the chain length increases at a diminishing rate. The optimization algorithm searches for improved fits, however as seen in Figure S3, the model fit the experimental MMA medium dispersity system data similarly

at a μ_{decap} of 10 and 30, although observable variation was found at a μ_{decap} of 3 or 5. Beyond a particular μ_{decap} value, the model's fit to the experiment undergoes minor variation. Overall, the model was able to accurately describe trends in dispersity both as the activity of the CTA was changed across a range of monomers, as well as for systems with mixed RAFT agents. For the mixed CTA systems, the model shows that k^* value is similar to the mole fraction average of the individual CTA k^* values.

Going beyond the thermal RAFT system, the applicability of the model to photoinitiated RAFT was also explored.[51] In this case, the PET-RAFT system[62, 63] was explored for the same two monomers, MA and MMA, except that the photocatalyst, Eosin Y, was used to generate radicals under mild visible light irradiation. The schematic representation of PET-RAFT polymerization is given in Scheme 2. Figure 4A and 4B demonstrate the excellent agreement between the experimental PET-RAFT SEC data and the model for both MA and MMA systems. As seen in Figure 4 and Table 1 the results of the PET-RAFT closely mimic those found in thermally initiated RAFT. The value of k^* increased as dispersity increased for both the PET-RAFT MA and MMA systems. Also, the μ_{decap} decreased as the dispersity of these systems increased. There is some variation in the values of k^* and μ_{decap} between the PET-RAFT of MA, but this is relatively small, and could be due to temperature effects. In the case of PMMA, the values of k^* were consistently smaller in PET-RAFT than in thermal system, although this difference was relatively minor in all but the narrow MMA PET-RAFT system. The consistency of the parameters, in particular k^*, obtained by thermally initiated RAFT and PET-RAFT indicate that the RAFT degenerative transfer mechanism dominates the control over polymer chain length and deactivation of radicals, even in PET-RAFT. This is consistent with the findings of Xu et al.[64] where a calculation showed that control by reversible termination was not feasible in single unit monomer insertion PET-

RAFT. Importantly, the analysis performed on PET-RAFT broadens the model's use against various RAFT systems, as well as identifying that degenerative transfer, not reversible termination, dominate control in PET-RAFT.

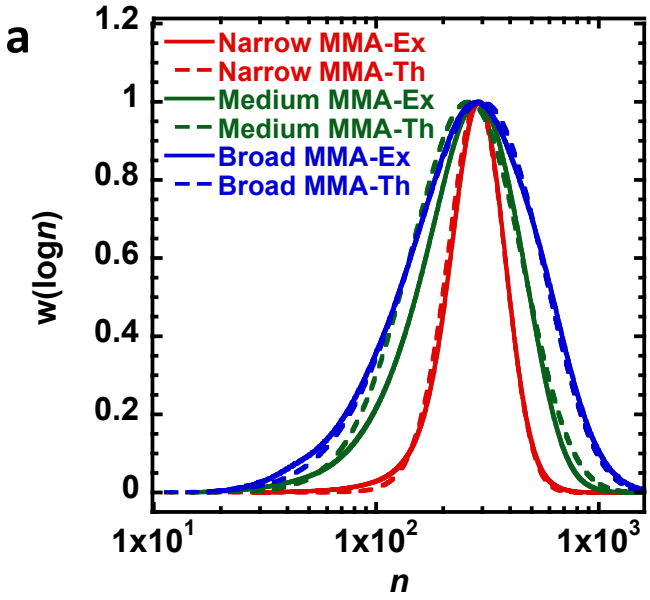

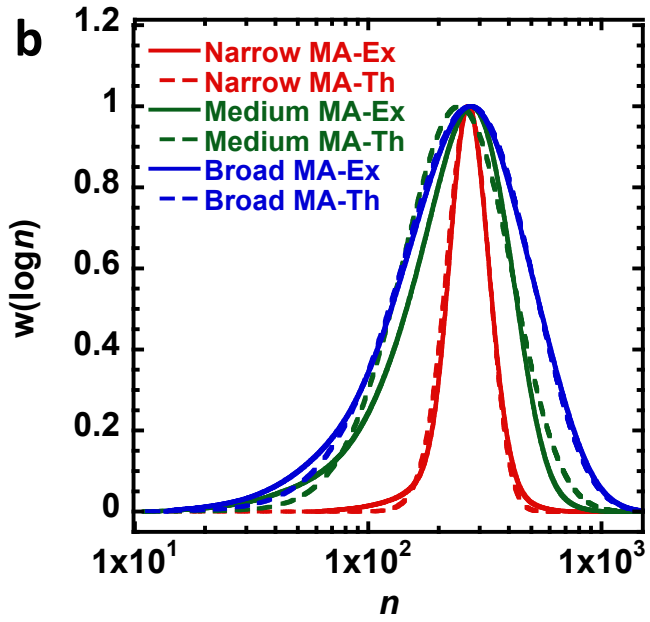

Figure 4. a) Molecular weight distributions from the PMMA PET-RAFT polymer system and model predictions. **b)** Molecular weight distributions from the PMA PET-RAFT polymer system and model predictions.

Application to ATRP reactions

In addition to RAFT polymerization, ATRP has emerged has a powerful tool to control polymers and molecular weight distributions. Using transition metal catalysts, the halogen-capped chain can be reversibly activated and deactivated to a propagating radical form, as shown in Equations 4 and 5. The deactivation occurs through the high oxidation state metal catalyst, and is decoupled from chain initiation, which occurs from the initially added alkyl halide. This offers the advantage of controlling the polymer chain dispersity by modulating the concentration of transition metal catalyst,[52, 65] rather than using a mixture of CTAs of different activities. As seen in Figure 5, the model can accurately capture the trend in the data as the catalyst loading is decreased. With lower catalyst loading, the distribution broadens and the dispersity increases, as seen in Table 1 and Figure 5. As expected with the lower catalyst loading, the transient radical lifetime increases, and therefore, to reach similar conversion and chain length to the systems with higher catalyst loading, the typical polymer undergoes fewer activation deactivation cycles. This results in lower μ_{decap} values, but more monomers are also added once the chain is activated. Ideally, the ratio of propagation to deactivation rate coefficients should be constant and independent of the catalyst loading. However, similar to the simpler dispersity-based analysis, variations in the k^*, or ratio of propagation to deactivation rate coefficients are found, with the k^* value increasing at the lower dispersity or higher catalyst loadings. One factor that could influence the observed values is that most polymer molecular weight distributions are determined by SEC, which is often affected by

band broadening.[66, 67] This additional dispersity may cause a relatively large broadening of narrow chains, while for highly disperse polymers the added breadth in the distribution is likely to be relatively small. Nevertheless, good fits to the ATRP synthesized polymers were possible with this approach.

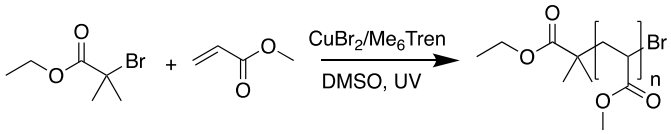

Scheme 3. ATRP photopolymerization of methyl acrylate using a $CuBr_2/Me_6TREN$ photocatalytic system.

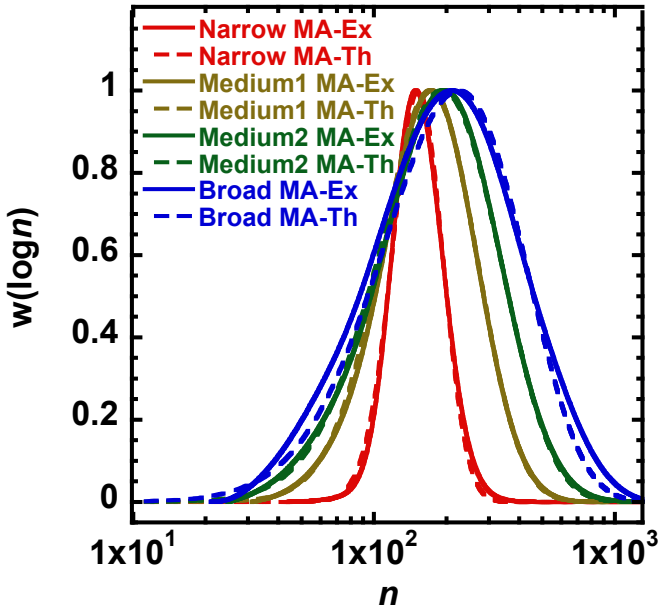

Figure 5. Molecular weight distributions from the PMA ATRP polymer system and model predictions.

Since deactivator and chain initiator concentrations can be independently varied in ATRP, it is, in principle, possible to reach higher dispersities by ATRP, simply by lowering the deactivator concentration, assuming there is sufficient chain activation to drive the reaction forward. To

explore this limit of chain dispersity possible, the deactivator concentration was changed in the context of the ATRP system described above. For the model to perform properly, the deactivation of the chain must dominate propagation. Thus, the ratio of $k^*\frac{[P-X]}{[D]}$ must be below one in the model. Figure S4 shows the molecular weight distribution produced when the ratio above is set to equal 0.99, or just below unity. If this ratio were to equal or exceed 1, deactivation no longer dominates propagation, and the model cannot function properly. In this case the polymer generated had a $Đ$ of 2.03 (1.97 if neglecting the unreacted initiating unit at chain length 1), simulated under the conditions μ_{decap} = 3.6, k*=0.0004. The results obtained here indicate that the model for the MWD can be expanded to ATRP and other systems with decoupled chain initiation and deactivation. The model was able to capture key trends in MWD obtained by varying the deactivator concentration, within limits of experimental methods.

Application of the model to cationic polymerizations

Cationic polymerization is also a technique that participates in reversible activation/deactivation processes of chain ends.[53] In the case of a recent cationic polymerization with tunable dispersity, the simplest model involves the chain end reversibly binding to a Lewis acid, creating an active chain end with cationic character. This chain end can add monomer, before reversibly deactivating through the unimolecular loss of the Lewis acid. As seen in Scheme 4, two distinct end groups can be accessed in this cationic polymerization, with one end group being 'open' DTE (O) and the other being 'closed' DTE (C). The open-DTE end group generally leads to higher dispersity than the closed-DTE end group.[53]

As seen in Figure 6, the auxiliary group (Z=OMe, H, or CN) can modulate the range of dispersities accessed. All systems have mean chain lengths close to the target of DP_n≈100. In

general, the open form leads to similar molecular weight distributions and dispersities in the order of $Đ$ = 1.25. However, the auxiliary group, X, leads to notable changes in the closed form, with the OMe group giving dispersities in the order of 1.17, followed by the H giving dispersities in the order of 1.15 while CN gave a dispersity of approximately 1.10. This is reflected in the k^* values obtained, with all open systems having large k^* values of ca. 70-80, while the closed system having k^* values that decreased from k^*=53, 37, and 24 for X=OMe, H, and CN, respectively (Table 1). A significant advantage of the general model developed here, is that it can be applied to a system with knowledge only of the chain length distribution and its moments, which give DP_n and $Đ$ to gain insights to the chain length distribution. This is especially useful in systems like cationic polymerization, where knowledge of the absolute rate coefficients is not always as well established as in radical polymerization, implying that tools which require minimal inputs can be used in such systems to gain important insights into the underlying process. The application of the model to cationic systems indicates the generality of the model towards systems with reversible activation. The studied cationic system identified trends in the control over MWD, and shows the generality of high k^* being correlated with broader MWDs, across a range of polymerization systems.

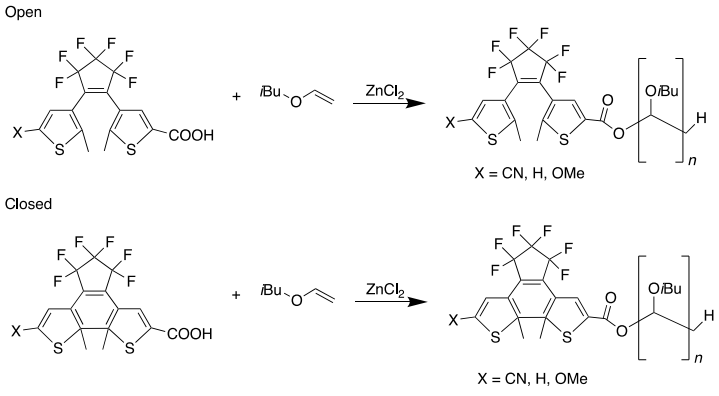

Scheme 4. Cationic polymerization scheme of isobutylvinylether using both open and closed DTE. X group is where substitution of substituents occurs (X= CN, H or OMe).

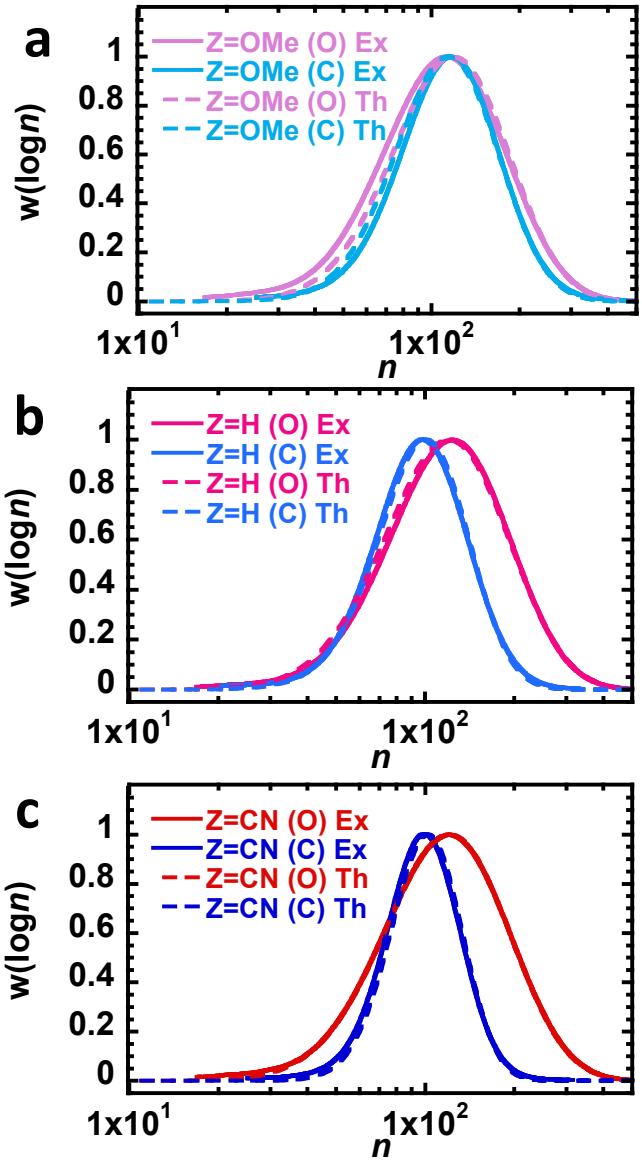

Figure 6. a) Data and model fit to OMe-DTE-COOH open and closed cationic polymer systems. **b)** Data and model fit to H-DTE-COOH open and closed cationic polymer systems. **b)** Data and model fit to CN-DTE-COOH open and closed cationic polymer systems.

Table 1. Summary of all experimental and fitted results studied in this system across RAFT, PET-RAFT, ATRP and cationic polymerization.

System	Label	[M]:[P-X]:[D]	k^*	μ_{decap}	$DP_{n\text{-}Ex}$	$Đ_{Ex}$	$DP_{n\text{-}Th}$	$Đ_{Th}$
RAFT MA	Narrow	300:1:1	0.058	32	230	1.09	260	1.05
	Medium	200:1:1	0.48	5.1	190	1.37	190	1.36
	Broad	200:1:1	0.64	2.6	180	1.63	180	1.64
RAFT MMA	Narrow	300:1:1	0.13	15	250	1.13	260	1.10
	Medium	200:1:1	0.56	30	200	1.39	200	1.39
	Broad	200:1:1	0.73	2.6	190	1.65	190	1.65
PET-RAFT MA	Narrow	300:1:1	0.084	36	280	1.10	290	1.05
	Medium	200:1:1	0.57	29	210	1.36	200	1.40
	Broad	200:1:1	0.69	7.3	210	1.51	200	1.53
PET-RAFT MMA	Narrow	300:1:1	0.060	20	210	1.09	220	1.07
	Medium	200:1:1	0.39	3.2	160	1.40	160	1.41
	Broad	200:1:1	0.59	1.9	160	1.71	160	1.76
ATRP	Narrow	150:1:0.02	0.0019	33	150	1.06	150	1.06
	Medium 1	150:1:0.002	0.00071	8.2	140	1.20	150	1.24
	Medium 2	150:1:0.001	0.00055	4.8	140	1.33	150	1.41
	Broad	150:1:0.0005	0.00047	3.6	140	1.48	150	1.64
Cationic	MeO-DTE-COOH (O)	0.5:0.005:1	74	55	94	1.26	100	1.23
	MeO-DTE-COOH (C)	0.5:0.005:1	59	54	100	1.17	100	1.18
	H-DTE-COOH (O)	0.5:0.005:1	82	56	100	1.25	100	1.26
	H-DTE-COOH (C)	0.5:0.005:1	37	10	91	1.15	89	1.14
	CN-DTE-COOH (O)	0.5:0.005:1	83	39	100	1.26	100	1.27
	CN-DTE-COOH (C)	0.5:0.005:1	24	22	110	1.10	95	1.08

Application to Complex Polymer Systems

Recently, polymers with tunable dispersities of exceptional precision could be generated by taking two polymers of distinct dispersities, but similar M_n values, and blending them together as demonstrated in Scheme 5.[57] For instance, polymers of low and high dispersity can be synthesized by ATRP, and the distribution approximated well by the model developed above. As seen in Figure 7, distributions of blended polymers can be predicted by combining the modelled narrow and broad distribution through a weighted summation, where the weighting is the fraction of broad and narrow polymer respectively.[57] The modelled blended polymers agree well with the experimentally evaluated distribution for the blended systems. As anticipated, systems with a higher ratio of the broad polymer also have broader distribution.

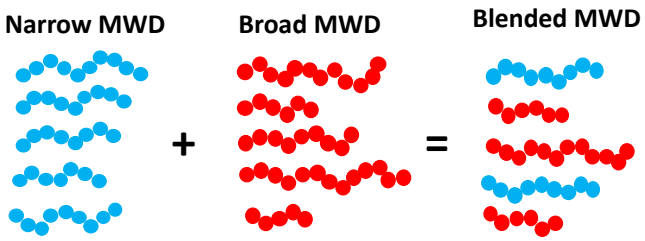

Scheme 5. Visual representation of a blending mechanism, where the narrow and broad MWD polymers are blended together in specific ratios.

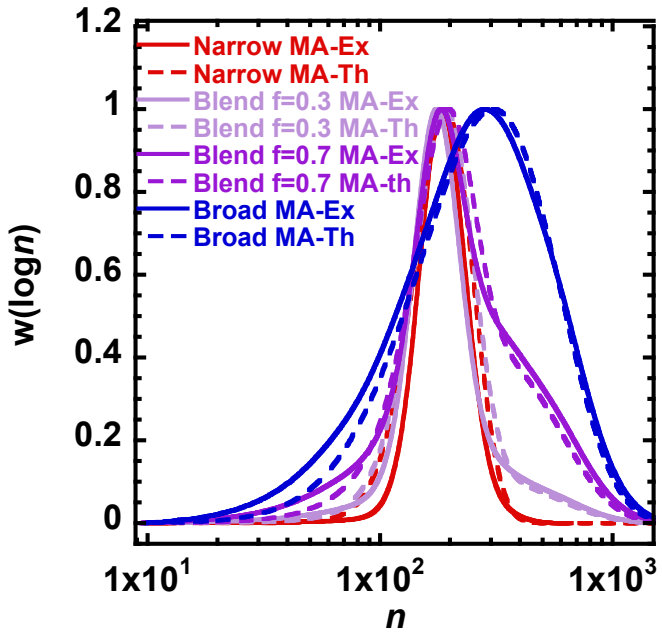

Figure 7. Data from a blended polymer system. P1 is a high dispersity polymer and P2 is a low dispersity polymer. Experiment and model are given for the narrow, the broad and blended polymers with a fraction of 0.3 or 0.7 of the broad distribution.

Finally, the approach developed through convolution is applied to block copolymer systems.[68] In describing block copolymers, each block is individually modelled, with the resulting two blocks convoluted using Equation 30. Additionally, since all the block copolymer systems studied were made by radical polymerization, there is a possibility of dead chains from the first

block. These can be treated as a blended system, with one polymer being treated as the living block polymer generated by convolution of the two individual chain length distributions, and the other being the dead chain, which can be approximated by the chain length distribution of the first block. As seen in Figure 8, the model can give good predictions of the homopolymers and block copolymer of 3 polymerization systems. The first is an ATRP polymer, where the first block of PMMA was chain extended with ethyl acrylate (EA).[55] Excellent agreement between the model and the experiment is seen in the PMMA homopolymer, and acceptable agreement is observed when considering the overall experimental block copolymer and the living chains, as seen in Figure 8a. However, including 4% of the PMMA homopolymer as dead chains improves the fit, especially at lower chain lengths. The parameters used to fit the two blocks are given in Table S4.

A similar result was observed in the RAFT block copolymerizatiom phenylvinylketone (PVK) and butyl acrylate (BA), as depicted in Figure 8b. Both blocks targeted 50 units. The PPVK homopolymer is described well by the model, and since the BA chain is similarly controlled, the theoretical distribution of BA chain lengths shown in yellow was similar to the PPVK block. The overall block copolymer is well-described by the model, although a notable fraction (11%) of the dead chains from PPVK were needed to describe the experimental molecular weight distribution. In ideal RAFT, the formation dead chains is correlated from new chains generated in the system, and therefore [P–X] should remain constant in ideal RAFT. Certain kinetic models, such as the intermediate radical termination model,[69, 70] do lead to decreases in the [P–X] from cross-termination reactions although this is beyond the scope of this model. It is important to note that the experimental PPVK-b-BA block copolymer molecular weight and chain length was corrected by the Mark-Houwink parameters for BA as derived by Barner-Kowoillik and co-workers.[71]

Additional discrepancies between model and experiment are likely to be caused by deviations between the solution dimensions of PMMA calibrants and the complex block copolymer.

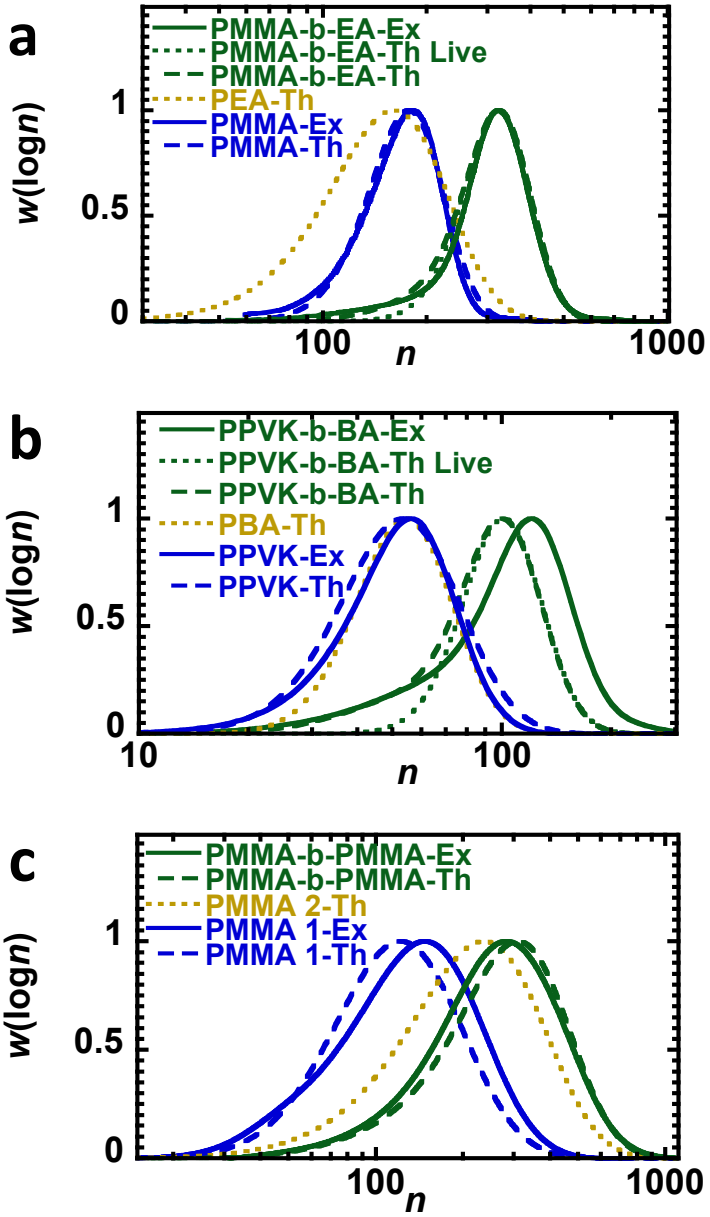

Figure 8: a) ATRP block copolymer of MMA and EA, b) RAFT block copolymer of PVK and BA, c) RAFT copolymer where the two blocks are both MMA. Blue describes the homopolymer or first block (experimental-solid and theoretical-dashed), yellow dotted gives the theoretical chain

length distribution of the second block, and green gives the block copolymer (experimental-solid, overall theoretical-dashed and only live block copolymer-dotted).

Finally, Figure 8c shows the mixed CTA chain extension of PMMA. The PMMA homopolymer was synthesized with 35% of the dithiobenzoate CTA which led to low dispersity and 65% of the CTA which leads to high dispersity. As seen in Table S4, the k^* value of 0.44 was obtained for the first block along with a μ_{decap} of 10. In order to fit the block copolymer, a substantially smaller k^* of 0.17 was required with μ_{decap} of only 1.4. Higher k^* values caused the peak of the molecular weight distribution to be shifted too high, due to the chain extension being performed with 400 equivalents of monomer cut off at a low conversion.[51] The likely reason for the substantially smaller k^* and μ_{decap} in the chain extension is the cessation of the reaction at low conversion, combined with the fact that some chain ends are capped with the more active dithiobenzoate, and others with the less active dithiocarbamate. RAFT exchange is most efficient through the dithiobenzoate groups, therefore the chains containing dithiobenozates are most likely to exchange and grow. This reduces the apparent k^* since chain extension is primarily occurring through the more active dithiobenzoates which will have lower k^* values. The low μ_{decap} is related to this, since the dithiocarbamate capped chains are less likely to have chain extended and therefore not all chains will have undergone multiple activation cycles. The application of the model against complex polymer systems such as blended and block structures show the versatility of the approach. In particular, the block polymer system shows how the overall block polymer MWD can be described as a convolution or combination of the individual MWDs, gaining information into the characteristics of each individual polymer distribution, in a way that is nearly impossible from a purely experimental perspective.

Conclusion

The model developed fits a range experimental data to two variables; k^* and μ_{decap}. μ_{decap} represents the average number of decapping events occur for a polymer chain and k^* represents the ratio of propagation to deactivation rate coefficients for the active chain. k^* is an important kinetic measure as well controlled polymerizations add only a few monomers per decapping cycle. Thus, the smaller the k^* value, the narrower the molecular weight distribution and the more uniform the chains will be. Interestingly, relatively well controlled chains, with dispersity in the order of 1.10 can be synthesized with μ_{decap} of 5, or 5 activation/deactivation cycles on average. Higher numbers of activation cycles will increase conversion and chain length, with a commensurate decrease in dispersity. The model was used to describe molecular weight distributions of polymers made by a variety of systems including ATRP, RAFT, PET-RAFT, and cationic polymerization. Importantly, the model was able to capture trends in dispersity by increasing k^* in RAFT and cationic systems or capturing the increase in dispersity through lower deactivator concentrations in ATRP. Additionally, the model could describe complex block and blended polymers, with good agreement between the model and the experimental data. The most substantial benefit of this model is its simplicity. It can be applied to most polymer systems subjected to reversible activation/deactivation, and with just the molecular weight distribution, the mean and molar mass dispersity, kinetic parameters, and history of the polymerization can be extracted for new polymer systems.

Theoretical Section and Model Derivation

In general, the model developed below applies to any process which involves a reversible activation-deactivation of polymer chain ends. In the dormant state, the monomers are unable to

react with the polymer chain, while in the active state, which is typically short-lived, monomers are added to the chain end. It is important to note that the methodology developed below applies to the living chains of a polymerization with intermittent activation and deactivation. Chains derived from irreversible transfer events or chains subjected to termination are not captured in the model. Therefore, the system is best applied to living-like polymers where the fraction of chains affected by transfer or termination is relatively small. In the following paragraphs, the general forms of RAFT, ATRP and cationic polymerization are outlined and summarized in terms of their activation, propagation and deactivation processes. Although the model is applied to cationic, RAFT and ATRP system, it could be used more broadly, including anionic or nitroxide mediated polymerization which can also show intermittent activation, propagation and deactivation.[72, 73] Subsequently, the model is derived in a general way such that it can be applied to any one of these or other polymerization systems.

In the case of RAFT polymerization, the deactivation occurs through degenerative exchange of thiocarbonylthio groups. This can be represented by equations 2 and 3 below, where $P_l^\bullet$ and $P_k^\bullet$ are propagating radicals and $P_k - X$ and $P_l - X$ are dormant chain transfer agent (CTA) capped chains. In this case both chain initiation and deactivation occur through the RAFT CTA. In this way, RAFT can be thought of as having simultaneous activation of a propagating radical, with deactivation of the propagating chain, assuming the RAFT intermediate radical is short lived.[74]

$$P_l^\bullet + P_k - X \xrightarrow{k_{RAFT}} P_l - X + P_k^\bullet \quad (2)$$

$$P_l - X + P_k^\bullet \xrightarrow{k_{RAFT}} P_l^\bullet + P_k - X \quad (3)$$

In the case of ATRP, the activation-deactivation equilibrium can be described by the processes below. The activation occurs from the Cu^I/L complex, or any other low-valent metal

capable of activating (pseudo)alkyl halides, while deactivation occurs by $X-Cu^{II}/L$ or any other high-valent metal capable of deactivating propagating radicals. These processes are given in Equations 4 and 5 below.[14]

$$P_k-X + M^n/L \xrightarrow{k_{a-ATRP}} P_k^{\bullet} + X - M^{n+1}/L \quad (4)$$

$$P_k^{\bullet} + X - M^{n+1}/L \xrightarrow{k_{d-ATRP}} P_k-X + M^n/L \quad (5)$$

Similarly, in the simplest case, reversible deactivation cationic polymerization can be thought of as a Lewis acid coordination-based activation of the propagating chain end. This can be captured by the processes in Equations 6 and 7 below:[53]

$$P_k-X + LA \xrightarrow{k_{a-CAT}} P_k^{\delta+}\text{–}X\text{–}LA \quad (6)$$

$$P_k^{\delta+}\text{–}X\text{–}LA \xrightarrow{k_{d-CAT}} P_k-X + LA \quad (7)$$

In general monomer propagation follows the pathways given in Equation 8 for radical reactions or Equation 9 for cationic reactions. Both processes follow the key ideas in addition polymerization.

$$P_k^{\bullet} + M \xrightarrow{k_p} P_{k+1}^{\bullet} \quad (8)$$

$$P_k^{\delta+}\text{–}X\text{–}LA + M \xrightarrow{k_p} P_{k+1}^{\delta+}\text{–}X\text{–}LA \quad (9)$$

In developing a general model for polymerization with intermittent polymer chain activation and deactivation, it is important to consider two factors: the mean number of activation cycles experienced by the chain-end and the number of monomers added in an activation cycle. The first factor is the mean number of chain-end activation cycles that the average polymer chain undergoes. In the model these are referred to as decapping cycles, wherein the chain cap is removed to produce an active chain end. This mean number of decapping events is given by μ_{decap}. Although there is a distribution of the number of decapping events per chain, each polymer will

have a unique number of activation or decapping cycles. The likelihood of a given polymer undergoing precisely *j* decapping events, is assumed to follow a Poisson distribution, with a mean μ_{decap} as given below:[49]

$$P_{decap}(j|\mu_{decap}) = \frac{\exp(-\mu_{decap})(\mu_{decap})^{j}}{j!} \quad (10)$$

Equation 10 holds regardless of the underlying polymerization mechanism. The Poisson distribution is applied here, as the decapping events are assumed to be independent of each other, with the Poisson distribution often being used to describe the probability of a given number of independent 'rare' events occurring in a given time frame, assuming the time to the next event, such as a decapping, is independent of the prior one.[75] In this case of a polymerization that would be the total polymerization time.

Upon polymer chain activation, monomers may be added to the system. Monomers will continue to be added with rate coefficient k_p until the chain is deactivated. In a well-controlled reaction, as is assumed to occur in the model, the dominant modes of chain deactivation are either reversible termination or degenerative transfer, with minimal irreversible chain ending events, such as irreversible chain transfer or irreversible termination. Following the deactivation steps in Equations 2, 3, 5, and 7 the mean number of monomers added during an activation cycle can be estimated as follows for RAFT, ATRP, and cationic processes, respectively, given a concentration of monomer [M]:[49]

$$\mu_{add} = \frac{k_p[M]}{k_{RAFT}[P_k - X]} \quad (11)$$

$$\mu_{add} = \frac{k_p[M]}{k_{d-ARTP}[X\text{–}M^{n+1}/L]} \quad (12)$$

$$\mu_{add} = \frac{k_p[M]}{k_{d-CAT}} \quad (13)$$

Note that in equation 11, $[P_j - X]$ is the concentration of thiocarbonylthio chain transfer agents, typically equal to the total concentration of RAFT agent added at the start of the reaction. In this way, the general format for the mean number of monomers added per activation-deactivation cycles is given by:

$$\mu_{add} = \frac{k_p[M]}{k_D[D]} \quad (14)$$

where $[M]$ is the monomer concentration at that deactivation, $[D]$ is the concentration of deactivating species, and k_D is the rate coefficient for deactivation. In the case of RAFT, deactivation occurs by reversible chain transfer; hence, $[D]$ is the initial concentration of RAFT agent and $k_D = k_{RAFT}$, while for ATRP the $[D]$ is the concentration of the high oxidation state deactivator and $k_D = k_{d-ATRP}$. In the case of cationic polymerization, deactivation has been proposed to occur by the loss of the Lewis acid, which occurs with rate coefficient $k_D = k_{d-CAT}$. Although there is no bimolecular deactivation in cationic polymerization, the unimolecular aspect can be captured by for by setting $[D]$=1 in eq 14 for cationic species, thereby transforming deactivation to a unimolecular process.

Given that the mean number of monomer units added for an activation-deactivation cycle is equal to μ_{add}, the probability of adding precisely *i* units during that activation-deactivation cycle can be given by the following distribution:[49]

$$P_{add}(i|\mu_{add}) = u^i(1-u) \quad (15)$$

Where:

$$u = \frac{\mu_{add}}{1+\mu_{add}} \quad (16)$$

The geometric distribution in equation 15 essentially accounts for the probability of adding *i* monomers before the deactivation or capping event. This models the probability of *i* independent

monomer addition events,[46] which each occur with probability u, before the successful recapping of the chain.

It is important to consider that as incorporation of monomer in an earlier activation-deactivation cycles across the population of all chains will deplete available monomer in subsequent decapping events for a given polymer. Given the living-like properties of the polymers, with linear growth of average chain length with conversion, this will cause μ_{add} to decrease as the polymerization progresses. In this way, the chain length after the average chain has experienced j decappings is given by:

$$DP_j = \frac{[M]_0 - [M]_j}{[P-X]} \quad (17)$$

Where $[M]_0$ is the initial monomer concentration, $[M]_j$ is the monomer concentration after the average chain has undergone j decapping events and $[P-X]$ is the concentration of active or living chain ends. Although this considers the typical or average chain and its effect on chain length and monomer concentration, which enables simplification of the calculation, there will be variations in the number of times different chains have been activated in a given timeframe.

In RAFT, $[P-X]$ is equal to the initial CTA concentration, assuming negligible degradation of the CTA; in ATRP $[P-X]$ is the alkyl halide concentration; and in cationic polymerizations $[P-X]$ is the concentration of cationic initiating groups. This enables the mean number of monomers added after the typical chain has undergone j decapping event to be written as shown in Equation 18.

$$\mu_{add,j} = \frac{k_p[M]_j}{k_D[D]} \quad (18)$$

Combining equation 18 with equation 17 gives:

$$\mu_{add,j} = \frac{k_p([M]_0 - DP_j[P-X])}{k_D[D]} \quad (19)$$

Recognizing that the polymer starts with chain length equal to 0, this equation can be solved to yield the general form below for the mean number of monomers added to a chain end ($\mu_{add,j}$), after the average chain has undergone *j* decappings:

$$\mu_{add,j}(k^*,[M]_0,[P-X],[D]) = k^* \frac{[M]_0}{[P-X]}\left(1 - k^* \frac{[P-X]}{[D]}\right)^{j-1} \quad (20)$$

Where k^* is the ratio of monomer addition to chain deactivation rate coefficients:

$$k^* = \frac{k_p}{k_D} \quad (21)$$

It is important to note that within the framework of the developed model, the ratio $k^* \frac{[P-X]}{[D]}$ must be less than 1. Although in principle the ratio can be greater than 1, this will lead to a system where only a few chains contain monomer, and most of the chain ends did not initiate efficiently.

Since the polymer initiates from a linear chain with one unit (the initiating unit) and zero monomer units incorporated. This gives the linear chain distribution of polymers with precisely 0 decapping cycles of:

$$P_{chain}(n|k^*,0,[M]_0,[P-X],[D]) = \begin{cases} 1 \ if \ n = 1 \\ 0 \ otherwise \end{cases} \quad (22)$$

Where *n* represents the chain length or degree of polymerization of the macromolecule. Note that this considers the initiating unit to be a macromolecule of chain length 1.

As the polymer chain undergoes subsequent decapping, or chain-end activation, events the linear chain length distribution grows by adding monomer. The probability of adding precisely *i* monomer units after *j* decapping cycles is given by $P_{add}(i|\mu_{add,j})$, as given in Equation 15. Therefore, after the average chain has undergone the j^{th} decapping, the probability of the linear polymer having exactly *n* units is given by the equation below:

$$P_{chain}(n \mid k^*,j,[M]_0,[P-X],[D])$$

$$= \sum_{i=0}^{n-1} P_{chain}(n-i|k^*,j-1,,[M]_0,[P-X],[D]) \times P_{add}(i|\mu_{add,j},[M]_0,[P-X],[D]) \quad (23)$$

The probability of finding a chain with length n after the j^{th} decapping is given by the sum of probability of finding a polymer with n unit in the prior decapping multiplied by the probability of adding no monomers in the j^{th} decapping, plus the probability of a chain having n–1 units multiplied by the probability of adding one monomer in the j^{th} decapping, plus the probability of a chain having n–2 units multiplied by the probability of adding two monomers in the j^{th} decapping, etc. Finally, to account for the fact that distinct polymers will have undergone different numbers of decapping cycles, the number distribution of polymer chain lengths, given a particular value of k^* and μ_{decap}, is given by adding the probability of a chain of length n being obtained after 0 decappings multiplied by the probability of the polymer undergoing 0 decappings, plus the probability of a chain of length n being obtained after 1 decappings multiplied by the probability of the polymer undergoing 1 decappings, etc. This yields the approximate solution to the polymers chain length distribution:

$$P_{CLD}\left(n|\mu_{decap},k^*,[M]_0,[P-X],[D]\right) =$$

$$\sum_{j=0}^{\infty} P_{decap}(j|\mu_{decap})\, P_{chain}(n|k^*,j,[M]_0,[P-X],[D]) \qquad (24)$$

This theoretical molecular chain length distribution is a function of two parameters of the model: μ_{decap} the mean number of decapping cycles; and k^* the ratio of propagation to deactivation rate coefficients; as well as three experimental parameters: $[M]_0$ the initial monomer concentration; $[P-X]$ the concentration of living chain ends; and $[D]$ the concentration of deactivator.

It is important to note that several simplifying assumptions were applied to derive equation 24. Firstly, the model focuses only on living chains, and assumes that chain ending transfer and termination are negligible, implying that most chains are living. A substantial fraction of dead chains would lead to broadening of the distribution that would not be captured by the model

without some modifications, as discussed in the section on block copolymers. Additionally, in deriving the model the number of monomers added in a given decapping was derived from the average monomer concentration after the typical chain underwent a set number of activation-deactivation cycles. This assumption neglects the fact that some chains may undergo more than the mean number of decapping events, and deplete monomer from chains that may have undergone fewer than the mean number of decapping events at a given point in the polymerization.

From the number distribution given in Equation 24, the mean chain length (DP_n) and the chain length dispersity (Đ) can be estimated as follows:

$$DP_n\left(\mu_{decap},k^*,[M]_0,[P-X],[D]\right)=\sum_{n=1}^{\infty}nP_{CLD}\left(n|\mu_{decap},k^*,[M]_0,[P-X],[D]\right) \quad (25)$$

$$Đ\left(\mu_{decap},k^*,[M]_0,[P-X],[D]\right)=\frac{\sum_{n=1}^{\infty}n^2P_{CLD}\left(n|\mu_{decap},k^*,[M]_0,[P-X],[D]\right)}{DP_n\left(\mu_{decap},k^*,[M]_0,[P-X],[D]\right)^2} \quad (26)$$

Finally, since most polymer distributions are measured by size exclusion chromatography (SEC), the SEC-based weight distribution can be calculated as follows:

$$w\left(logn\,\middle|\,\mu_{decap},k^*,[M]_0,[P-X],[D]\right)$$

$$=\frac{1}{C}\left(n^2\times P_{CLD}\left(n|\mu_{decap},k^*,[M]_0,[P-X],[D]\right)\right) \quad (27)$$

Where C is a normalization factor, either the peak value of $w(logn|\mu_{decap},k^*,[M]_0,[P-X],[D])$ to normalize to a height of 1, or the area under $w(logn|\mu_{decap},k^*,[M]_0,[P-X],[D])$ to give area normalized $w(logn|\mu_{decap},k^*,[M]_0,[P-X],[D])$. Additionally, a number distribution in log chain length (log n) can be represented as shown below:

$$p(logn|\mu_{decap},k^*,[M]_0,[P-X],[D])=\frac{1}{E}\left(n\times P_{CLD}\left(n|\mu_{decap},k^*,[M]_0,[P-X],[D]\right)\right) \quad (28)$$

Where E is a normalization factor, either the peak value of $p(logn|\mu_{decap},k^*,[M]_0,[P-X],[D])$ to normalize to a height of 1, or the area under $p(logn|\mu_{decap},k^*,[M]_0,[P-X],[D])$ to give area normalized $p(logn|\mu_{decap},k^*,[M]_0,[P-X],[D])$.

To fit an experimental SEC data set to the model, 3 parameters are considered and equally balanced: the mean chain length (DP_n), the dispersity ($Đ$), and the overall shape of the molecular weight distribution ($w(\log n)$). Considering all three parameters: DP_n; $Đ$; and $w(\log n)$, in the optimization reduces the sensitivity to experimental noise in any one parameter. Therefore, when optimizing against an experimental data set the following χ^2 parameter is minimized by optimization of k^* and μ_{decap}.

$$\chi^2(\mu_{decap},k^*) = \frac{\left(DP_{n-Ex}-DP_{n-Th}(\mu_{decap},k^*,[M]_0,[P-X],[D])\right)^2}{(DP_{n-Ex})^2} + \frac{\left(Đ_{Ex}-Đ_{Th}(\mu_{decap},k^*,[M]_0,[P-X],[D])\right)^2}{(Đ_{Ex})^2} + \frac{\sum_{i=1}^{n_{max}}\left(w_{ex}(logi)-w_{th}(logi|\mu_{decap},k^*,[M]_0,[P-X],[D])\right)^2}{\sum_{i=1}^{n_{max}}(w_{ex}(logi))^2} \quad (29)$$

Where i is each available experimental data point in the SEC derived chain length distribution up to the final chain length available (n_{max}). To make the system numerically tractable, the infinite summations in the number of decappings and chain length are capped. The maximum chain length considered in numerical calculations is taken as 20 times the ratio of $[M]_0$ to [P–X], or 20 times the targeted chain length. The maximum number of decappings is taken to be nearest integer to $\mu_{decap}+5\mu_{decap}^{0.5}$. This is corresponds to μ_{decap} + 5 standard deviations of the Poisson distribution.

Finally, when combining two existing chain length distributions, such as in a block copolymer or a polymer made of mixed RAFT agents, a convolution approach can be used as given below:

$$P_{con}\left(n \middle| \mu_{decap,1},\mu_{decap,2},k_1^*,k_2^*,[M]_{0,1},[M]_{0,2},[P-X]_1,[P-X]_2,[D]_1,[D]_2\right) =$$

$$\sum_{i=1}^{n} P_1(n-i+1|\mu_{decap,1},k_1^*,[M]_{0,1},[P-X]_1,[D]_1)P_2(i|\mu_{decap,2},k_2^*,[M]_{0,2},[P-X]_2,[D]_2) \quad (30)$$

Where $P_1(\mu_{decap,1},k_1^*,[M]_{0,1},[P-X]_1,[D]_1)$ and $P_2(\mu_{decap,2},k_2^*,[M]_{0,2},[P-X]_2,[D]_2)$ are the constituent polymer (number) chain length distributions with the parameters having the same

meaning as in equation 24. Note that this convolution approach is distinct from a blending approach, where blending two polymers P_1 and P_2 in fraction f by and $1\text{-}f$ is given by:

$$P_{blend}\left(n \middle| \mu_{decap,1},\mu_{decap,2},k_1^*,k_2^*,[M]_{0,1},[M]_{0,2},[P-X]_1,[P-X]_2,[D]_1,[D]_2\right) =$$

$$f\,P_1(n|\mu_{decap,1},k_1^*,[M]_{0,1},[P-X]_1,[D]_1)\;+\;(1-f)\,P_2(n|\mu_{decap,2},k_2^*,[M]_{0,2},[P-X]_2,[D]_2) \qquad (31)$$

The convolved or blended distribution can be then transformed to a weight distribution for comparison with SEC by applying the same approach as given in equation 27.

Acknowledgements

This work was partially supported by the National Science Foundation under Grant No. (DMR- 1749730) to D.K for PVK polymer synthesis, model development and validation. 400 MHz NMR instrumentation is supported through funding from the National Science Foundation under grant number (CHE- 1919850). D.K. acknowledges support from Miami University through the Robert H and Nancy J Blayney Professorship. Colleen Morley acknowledges support from Miami University through the College of Arts and Science Dean's scholar program for supporting model scope evaluation. A. A. gratefully acknowledges ETH Zurich for financial support of RAFT and ATRP experiments. K.P. thanks Onasis Foundation as this scientific paper was partially supported by the Onassis Foundation - Scholarship ID: FZQ051-1/2020-2021 for PET-RAFT systems. M.C. acknowledges the National Science Foundation CAREER Award (CHE-1945271) and A.D.S. acknowledges the Stony Brook University Department of Chemistry Graduate Research Award for financial support of the cationic systems.

Author Contributions

The model was developed and applied to polymer systems by D.K., C.N.M, and M.M.K. and P.C. and N.D.A.W. A.S. and M.C. were involved in application to and interpretation of cationic polymerizations. R.W. K.P. and A.A. were involved in application to and interpretation of

ATRP, RAFT and PET-RAFT systems. N.D.A.W. was involved in PVK based polymers. All authors were involved in editing and writing the manuscript.

Conflicts of Interest

The authors declare no conflicts.

Supplementary Information Available

Experimental details for PVK-BA block copolymers. Additional distributions and convolution analysis and blended polymer analysis. MATLAB Codes used to implement the model.

References

1 A. Goto, T. Fukuda, *Prog Polym Sci* 2004, **29**, 329.
2 K. Parkatzidis, H. S. Wang, N. P. Truong, A. Anastasaki, *Chem* 2020, **6**, 1575.
3 K. Matyjaszewski, C.-H. Lin, *Makromol Chem. Macromol Symp* 1991, **47**, 221.
4 M. Kamigaito, M. Sawamoto, *Macromolecules* 2020, **53**, 6749.
5 R. Whitfield, N. P. Truong, D. Messmer, K. Parkatzidis, M. Rolland, A. Anastasaki, *Chem Sci* 2019, **10**, 8724.
6 S. Domanskyi, D. T. Gentekos, V. Privman, B. P. Fors, *Polym Chem* 2020, **11**, 326.
7 D. J. Walsh, D. A. Schinski, R. A. Schneider, D. Guironnet, *Nat Commun* 2020, **11**, 3094.
8 S. K. Fierens, S. Telitel, P. H. M. Van Steenberge, M.-F. Reyniers, G. B. Marin, J.-F. Lutz, D. R. D'hooge, *Macromolecules* 2016, **49**, 9336.
9 P.-G. De Gennes, P.-G. Gennes, *Scaling concepts in polymer physics*, Cornell university press, **1979**.
10 M. Muthukumar, S. F. Edwards, *Polymer* 1982, **23**, 345.
11 M. R. Wood, D. J. Duncalf, P. Findlay, S. P. Rannard, S. Perrier, *Aust J Chem* 2007, **60**, 772.
12 Y. K. Chong, J. Krstina, T. P. T. Le, G. Moad, A. Postma, E. Rizzardo, S. H. Thang, *Macromolecules* 2003, **36**, 2256.
13 P. N. Kurek, A. J. Kloster, K. A. Weaver, R. Manahan, M. L. Allegrezza, N. De Alwis Watuthanthrige, C. Boyer, J. A. Reeves, D. Konkolewicz, *Ind Eng Chem Res* 2018, **57**, 4203.
14 K. Matyjaszewski, J. Xia, *Chem Rev* 2001, **101**, 2921.
15 T. Pintauer, K. Matyjaszewski, *Chem Soc Rev* 2008, **37**, 1087.
16 N. V. Tsarevsky, K. Matyjaszewski, *Chem Rev* 2007, **107**, 2270.
17 K. Matyjaszewski, W. Jakubowski, K. Min, W. Tang, J. Huang, W. A. Braunecker, N. V. Tsarevsky, *Proc Nat Acad Sci* 2006, **103**, 15309.
18 H. Tobita, A. E. Hamielec, *Macromolecules* 1989, **22**, 3098.
19 M. Wulkow, M. Busch, T. P. Davis, C. Barner-Kowollik, *J Polym Sci Part A: Polym Chem* 2004, **42**, 1441.
20 P. B. Zetterlund, G. Gody, S. Perrier, *Macromol Theory Simul* 2014, **23**, 331.

21 W. Tang, K. Matyjaszewski, *Macromol Theory Simul* 2008, **17**, 359.
22 P. Krys, H. Schroeder, J. Buback, M. Buback, K. Matyjaszewski, *Macromolecules* 2016, **49**, 7793.
23 E. Mastan, S. Zhu, *Eur Polym J* 2015, **68**, 139.
24 Y.-N. Zhou, Z.-H. Luo, *Macromol React Eng* 2016, **10**, 516.
25 D. R. D'Hooge, M. Fantin, A. J. D. Magenau, D. Konkolewicz, K. Matyjaszewski, *React Chem Eng* 2018, **3**, 866.
26 M. Zhong, Y. Wang, P. Krys, D. Konkolewicz, K. Matyjaszewski, *Macromolecules* 2013, **46**, 3816.
27 D. Konkolewicz, P. Krys, J. R. Góis, P. V. Mendonça, M. Zhong, Y. Wang, A. Gennaro, A. A. Isse, M. Fantin, K. Matyjaszewski, *Macromolecules* 2014, **47**, 560.
28 T. G. Ribelli, D. Konkolewicz, S. Bernhard, K. Matyjaszewski, *J Am Chem Soc* 2014, **136**, 13303.
29 D. Konkolewicz, B. S. Hawkett, A. Gray-Weale, S. Perrier, *Macromolecules* 2008, **41**, 6400.
30 M. J. Monteiro, *J Polym Sci Part A: Polym Chem* 2005, **43**, 3189.
31 D. J. G. Devlaminck, P. H. M. Van Steenberge, M.-F. Reyniers, D. R. D'hooge, *Polymers* 2019, **11**.
32 N. De Rybel, P. H. M. Van Steenberge, M.-F. Reyniers, C. Barner-Kowollik, D. R. D'Hooge, G. B. Marin, *Macromol Theory Simul* 2017, **26**, 1600048.
33 P. Vana, T. P. Davis, C. Barner-Kowollik, *Macromol Theory Simul* 2002, **11**, 823.
34 I. Zapata-Gonzalez, R. A. Hutchinson, M. Buback, A. Rivera-Magallanes, *Chem Eng J* 2021, **415**, 128970.
35 M. Drache, G. Schmidt-Naake, M. Buback, P. Vana, *Polymer* 2005, **46**, 8483.
36 D. Konkolewicz, Y. Wang, M. Zhong, P. Krys, A. A. Isse, A. Gennaro, K. Matyjaszewski, *Macromolecules* 2013, **46**, 8749.
37 C.-H. Peng, M. Zhong, Y. Wang, Y. Kwak, Y. Zhang, W. Zhu, M. Tonge, J. Buback, S. Park, P. Krys, D. Konkolewicz, A. Gennaro, K. Matyjaszewski, *Macromolecules* 2013, **46**, 3803.
38 Y. Wang, M. Zhong, W. Zhu, C.-H. Peng, Y. Zhang, D. Konkolewicz, N. Bortolamei, A. A. Isse, A. Gennaro, K. Matyjaszewski, *Macromolecules* 2013, **46**, 3793.
39 M. L. Coote, *Macromolecules* 2004, **37**, 5023.
40 M. L. Coote, E. H. Krenske, E. I. Izgorodina, *Macromol Rapid Commun* 2006, **27**, 473.
41 M. L. Coote, L. Radom, *J Am Chem Soc* 2003, **125**, 1490.
42 C. Fang, M. Fantin, X. Pan, K. de Fiebre, M. L. Coote, K. Matyjaszewski, P. Liu, *J Am Chem Soc* 2019, **141**, 7486.
43 C. Y. Lin, M. L. Coote, A. Petit, P. Richard, R. Poli, K. Matyjaszewski, *Macromolecules* 2007, **40**, 5985.
44 M. Edeleva, P. H. M. Van Steenberge, M. K. Sabbe, D. R. D'hooge, *Polymers* 2021, **13**.
45 H. Tobita, *Macromol Theory Simul* 2006, **15**, 12.
46 H. Tobita, *Macromol React Eng* 2008, **2**, 371.
47 A. Goto, T. Fukuda, *Macromolecules* 1997, **30**, 4272.
48 S. Harrisson, *Polymers* 2018, **10**.
49 D. Konkolewicz, M. Siauw, A. Gray-Weale, B. S. Hawkett, S. Perrier, *J Phys Chem B* 2009, **113**, 7086.

50 R. Whitfield, K. Parkatzidis, N. P. Truong, T. Junkers, A. Anastasaki, *Chem* 2020, **6**, 1340.
51 K. Parkatzidis, N. P. Truong, M. N. Antonopoulou, R. Whitfield, D. Konkolewicz, A. Anastasaki, *Polym Chem* 2020, **11**, 4968.
52 R. Whitfield, K. Parkatzidis, M. Rolland, N. P. Truong, A. Anastasaki, *Angew Chem Ind Ed* 2019, **58**, 13323.
53 D. Liu, A. D. Sponza, D. Yang, M. Chiu, *Angew Chem Ind Ed* 2019, **58**, 16210.
54 N. P. Truong, G. R. Jones, K. G. E. Bradford, D. Konkolewicz, A. Anastasaki, *Nat Rev Chem* 2021, **5**, 859.
55 D. Konkolewicz, K. Schröder, J. Buback, S. Bernhard, K. Matyjaszewski, *ACS Macro Lett* 2012, **1**, 1219.
56 N. De Alwis Watuthanthrige, J. A. Reeves, M. T. Dolan, S. Valloppilly, M. B. Zanjani, Z. Ye, D. Konkolewicz, *Macromolecules* 2020, **53**, 5199.
57 R. Whitfield, N. Truong, A. Anastasaki, *Angew Chem Ind Ed* 2021, **60**, 19383.
58 J. L. Baumgarten, J. P. Busnel, G. R. Meira, *J Liq Chromatogr Related Technol* 2002, **25**, 1967.
59 D. Konkolewicz, J. W. Taylor, P. Castignolles, A. Gray-Weale, R. G. Gilbert, *Macromolecules* 2007, **40**, 3477.
60 Y. W. Marien, M. Edeleva, F. L. Figueira, F. J. Arraez, P. H. M. Van Steenberge, D. R. D'Hooge, *Macromol Theory Simul* 2021, **30**, 2100008.
61 S. Harrisson, *Polym Chem* 2018, **9**, 1366.
62 M. L. Allegrezza, D. Konkolewicz, *ACS Macro Lett* 2021, **10**, 433.
63 J. Phommalysack-Lovan, Y. Chu, C. Boyer, J. Xu, *Chem Commun* 2018, **54**, 6591.
64 J. Xu, C. Fu, S. Shanmugam, C. J. Hawker, G. Moad, C. Boyer, *Angew Chem Ind Ed* 2017, **56**, 8376.
65 A. Plichta, M. Zhong, W. Li, A. M. Elsen, K. Matyjaszewski, *Macromol Chem Phys* 2012, **213**, 2659.
66 A. Goyon, D. Guillarme, S. Fekete, *J Pharm Biomed Anal* 2017, **135**, 50.
67 S.-T. Popovici, W. T. Kok, P. J. Schoenmakers, *J Chromatogr A* 2004, **1060**, 237.
68 M. J. Monteiro, *J Polym Sci Part A: Polym Chem* 2005, **43**, 5643.
69 G. Moad, *Macromol Chem Phys* 2014, **215**, 9.
70 K. G. E. Bradford, L. M. Petit, R. Whitfield, A. Anastasaki, C. Barner-Kowollik, D. Konkolewicz, *J Am Chem Soc* 2021, **143**, 17769.
71 T. Gruendling, T. Junkers, M. Guilhaus, C. Barner-Kowollik, *Macromol Chem Phys* 2010, **211**, 520.
72 D. Kunkel, A. H. E. Müller, M. Janata, L. Lochmann, *Makromol Chem. Macromol Symp* 1992, **60**, 315.
73 J. Nicolas, Y. Guillaneuf, C. Lefay, D. Bertin, D. Gigmes, B. Charleux, *Prog Polym Sci* 2013, **38**, 63.
74 S. Perrier, *Macromolecules* 2017, **50**, 7433.
75 C. Forbes, M. Evans, N. Hastings, B. Peacock, in *Statistical Distributions* (Eds.: C. Forbes, M. Evans, N. Hastings, B. Peacock), **2010**, p. https://doi.org/10.1002/9780470627242.ch35.